

pubs.acs.org/JPCL Letter

Extending the Large Molecule Limit: The Role of Fermi Resonance in Developing a Quantum Functional Group

Guo-Zhu Zhu,* Guanming Lao, Claire E. Dickerson, Justin R. Caram, Wesley C. Campbell, Anastassia N. Alexandrova, and Eric R. Hudson



Cite This: *J. Phys. Chem. Lett.* 2024, 15, 590–597



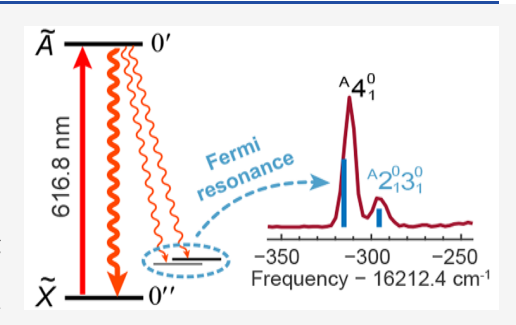
ACCESS I

Metrics & More

Article Recommendations

s Supporting Information

ABSTRACT: Polyatomic molecules equipped with optical cycling centers (OCCs), enabling continuous photon scattering during optical excitation, are exciting candidates for advancing quantum information science. However, as these molecules grow in size and complexity, the interplay of complex vibronic couplings on optical cycling becomes a critical but relatively unexplored consideration. Here, we present an extensive exploration of Fermi resonances in large-scale OCC-containing molecules using high-resolution dispersed laser-induced fluorescence and excitation spectroscopy. These resonances manifest as vibrational coupling leading to intensity borrowing by combination bands near optically active harmonic bands, which require additional repumping lasers for effective optical cycling. To mitigate these effects, we explore altering the vibrational energy level



spacing through substitutions on the phenyl ring or changes in the OCC itself. While the complete elimination of vibrational coupling in complex molecules remains challenging, our findings highlight significant mitigation possibilities, opening new avenues for optimizing optical cycling in large polyatomic molecules.

unctionalizing large molecules with optical cycling centers (OCCs) is being explored as a means for extending the exquisite control available in quantum information science to the chemical domain. 1-15 Success requires that these OCCs absorb and emit many photons without changing their vibrational states. To accomplish this task, molecular design rules are being developed, aided and validated by experiments, to guide the creation of the ideal quantum functional groups. 15-18 For example, prior work has demonstrated that alkaline earth alkoxides provide a general and versatile chemical moiety for optical cycling applications, as the alkaline earth radical electron can be excited without perturbing the vibrational structure of the molecule. 10,11,15-17 Similarly, traditional physical organic principles, such as electronwithdrawing, have been shown to improve OCCs performance.^{8,15} Further, experimental and theoretical extensions to more complex acenes, 9,16 diamondoids, 12 and even surfaces 19 suggest an exciting path forward for creating increasingly complex and functional quantum systems.

However, an open question for this work is what role will intramolecular vibrational energy redistribution (IVR) play as the molecule size is further increased? In the typical description of IVR, the normal modes of molecular vibrations are treated within the harmonic approximation, while any anharmonic couplings between these modes are treated as a perturbation. Laser excitation to an excited (harmonic) vibrational state is then followed by a redistribution of the vibrational energy driven by the anharmonic couplings. This outflow of energy from one vibrational mode to other modes

arises from the selection of basis states that are not eigenstates of the molecular Hamiltonian and thus not stationary.

An alternate and equivalent description of IVR takes the vibrational eigenstates of the molecular Hamiltonian as the basis. These basis states are mixtures of the harmonic vibrational modes with amplitudes set by the anharmonic couplings. As these states are eigenstates of the molecular Hamiltonian they are, of course, not time-evolving (except for their coupling to the electromagnetic vacuum), and therefore, there is no energy redistribution between them unless perturbed by an external field or collision. Instead, the effect of IVR in this picture is simply that there is more than one vibronic state within the spectrum of the exciting laser leading to nonexponential fluorescence as decay from these nearby states interfere.

This latter picture is convenient for understanding the role that IVR will play in functionalizing large molecules with OCCs. If harmonic vibrational states are close together and possess the correct symmetry, then anharmonic couplings will mix them. In this case, a harmonic vibrational state that is initially not optically active becomes optically active by mixing

Received: November 12, 2023
Revised: December 18, 2023
Accepted: December 21, 2023
Published: January 10, 2024





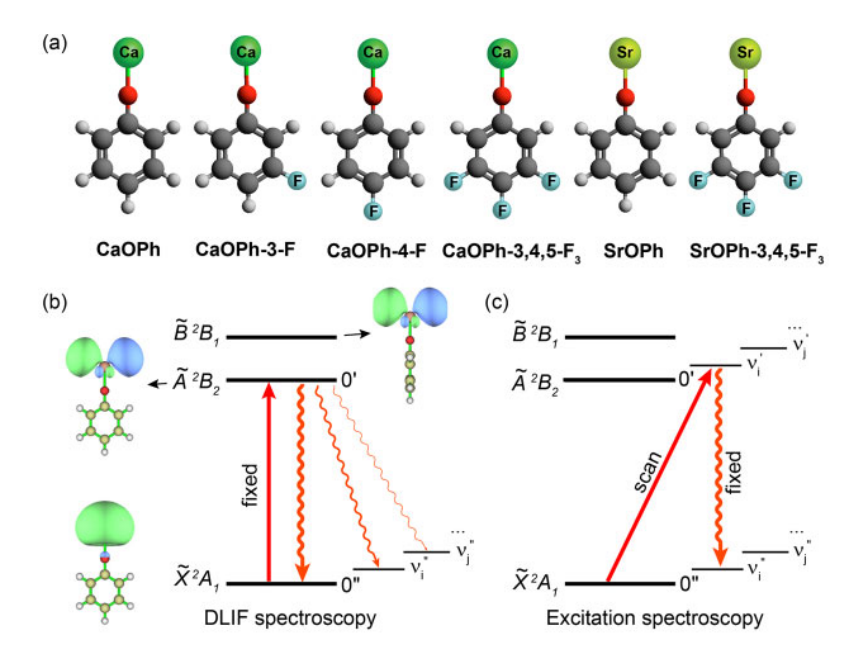


Figure 1. (a) Molecular structures of all studied calcium and strontium phenoxide and derivatives. (b, c) Schematic diagrams illustrating the DLIF measurement and excitation spectroscopy performed for all molecules in this study, respectively. DLIF measurements were performed by fixing the laser wavelength at the transitions of $\tilde{A}/\tilde{B}(v'=0) \leftarrow \tilde{X}(v''=0)$ and detecting the dispersed fluorescence. Excitation spectroscopy was carried out with off-diagonal excitation scan, $\tilde{A}/\tilde{B}(v'_n) \leftarrow \tilde{X}(v''=0)$, and diagonal fluorescence detection $\tilde{A}/\tilde{B}(v'_n) \rightarrow \tilde{X}(v''_n)$. The molecular orbital and symmetries of the electronic states are based on the CaOPh molecule with $C_{2\nu}$ symmetry.

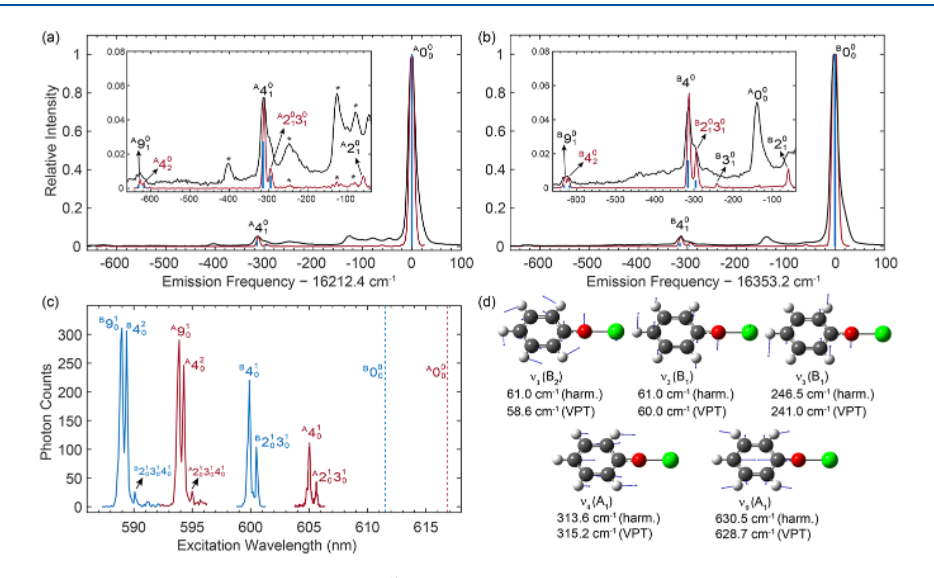


Figure 2. (a, b) Dispersed fluorescence spectra obtained for the $\tilde{A} \to \tilde{X}$ and $\tilde{B} \to \tilde{X}$ transitions of CaOPh. The black traces, adopted from previous work, ¹⁵ were obtained with a spectral resolution of ≈ 0.5 nm. The red traces come from an improved measurement with a resolution of ≈ 0.20 nm. The insets display the weak peaks in the range of -660 cm⁻¹ to -40 cm⁻¹ and show the presence of doublet peaks around -300 cm⁻¹ and -630 cm⁻¹. The blue sticks depict the calculated frequencies and relative strengths (FCFs) of the vibrational modes using the VPT method. The symbol *indicates CaOH contamination. (c) Excitation spectrum of the $\tilde{A}(\nu'_n) \leftarrow \tilde{X}(\nu''=0)$ (red traces) and $\tilde{B}(\nu'_n) \leftarrow \tilde{X}(\nu''=0)$ (blue traces) transitions. The resulting fluorescence is monitored on diagonal decays. The two dashed lines indicate the excitation wavelengths corresponding to the 0–0 transitions. The assignments of all observed vibrational resonances are given. (d) Vibrational displacements of five related fundamental modes. The symmetries and theoretical frequencies in \tilde{X} using harmonic and VPT methods are provided. All vibrational modes are labeled with increasing frequency, regardless of their symmetries.

with an optically active harmonic mode. While this does not change the fraction of diagonal decays ($\Delta \nu = 0$, where ν is the number of quanta in a vibrational mode), it does change the number of accessible final vibrational states and requires more repumping lasers to achieve optical cycling. ^{23–25}

Therefore, to push optical cycling to larger and larger molecules, it is desirable to develop molecular design principles

for avoiding these vibrational couplings by energy separation and/or symmetry. Here, we explore these phenomena in both the calcium and strontium phenoxides, which have recently been shown as promising candidates for optical cycling. ^{15,17,26} We show that in certain derivatives of these molecules it is possible to find combination modes (within the harmonic approximation), which are not themselves optically active,

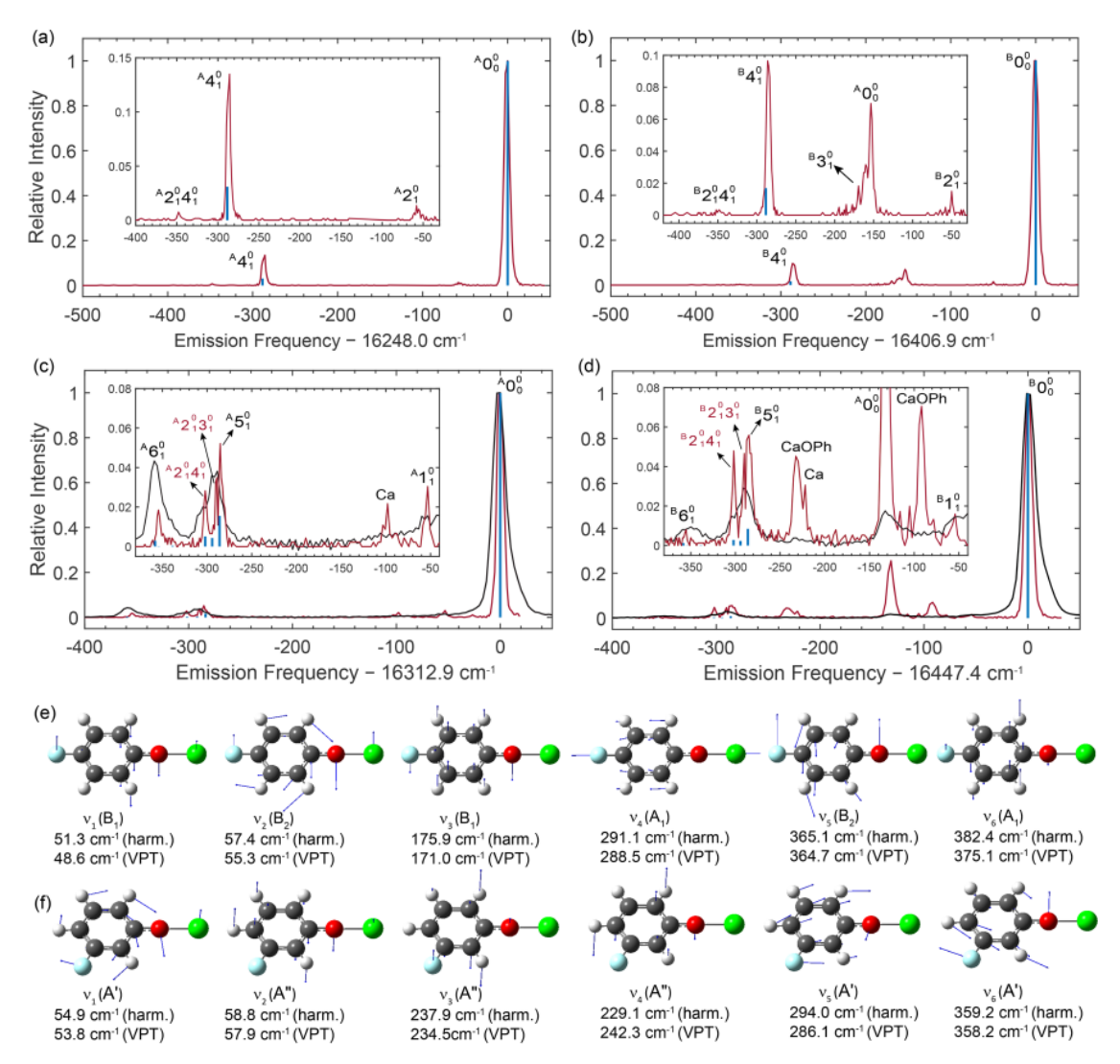


Figure 3. (a, b) Dispersed spectra for the $\tilde{A} \to \tilde{X}$ and $\tilde{B} \to \tilde{X}$ transitions of the CaOPh-4-F molecule, respectively. Only a single peak is observed for the stretching mode ν_4 around $-286~{\rm cm}^{-1}$. Due to the absence of Fermi resonance coupling, the theoretical relative strengths (blue vertical lines) are calculated under harmonic approximation. (c, d) Dispersed spectra for the $\tilde{A} \to \tilde{X}$ and $\tilde{B} \to \tilde{X}$ transitions of CaOPh-3-F molecule, respectively. The black traces are taken from previous work, ¹⁵ measured with a spectral resolution of \approx 0.5 nm, while the red traces represent improved measurements with a resolution of \approx 0.20 nm. Three decays near $-290~{\rm cm}^{-1}$ are observed. The blue vertical lines indicate the calculated vibrational frequencies and relative strengths using the VPT method. (e, f) Vibrational displacements of the six lowest-frequency fundamental modes in the ground state. Theoretical frequencies and symmetries for these modes are given. All vibrational modes are labeled with increasing frequency regardless of their symmetries.

close to optically active stretching modes. Anharmonic coupling between these modes—e.g., Fermi resonance, ^{27,28} which is the simplest instance of IVR—leads to intensity borrowing and the activation of the combination mode so that a new decay pathway is opened. Such molecules will require extra repumping lasers for optical cycling. By comparing phenoxides with and without this effect, we present further design rules for functionalizing ever larger molecules with optical cycling centers.

A series of calcium and strontium phenoxides (CaOPh, CaOPh-3-F, CaOPh-4-F, CaOPh-3,4,5-F₃, SrOPh, and SrOPh-3,4,5-F₃, Ph = phenyl group, Figure 1a) were produced via laser ablation of the alkaline earth metal into a mixture of the precursor ligand and Ne buffer gas inside a cryogenic cell operated at a temperature of \sim 20 K (Figure S1). ¹⁷ As sketched in Figures 1b and 1c, the vibrational structure of these molecules was probed with two types of measurements:

dispersed laser-induced fluorescence (DLIF) spectroscopy, which probes the vibrational structure in the electronic ground state (\tilde{X}) , and excitation spectroscopy, which examines the vibrational structure in the excited states (\tilde{A} and \tilde{B}). In DLIF spectroscopy (Figure 1b), vibrationally cold molecules are excited to the ground vibrational level of the electronically excited \tilde{A} and \tilde{B} states, $\tilde{A}/\tilde{B}(\nu'=0) \leftarrow \tilde{X}(\nu''=0)$, and the resulting fluorescence is recorded as a function of wavelength. In excitation spectroscopy (Figure 1c), the exciting laser is tuned to drive excitation to excited vibrational levels of the excited \tilde{A} and \tilde{B} states, $\tilde{A}/\tilde{B}(v'_n) \leftarrow \tilde{X}(v'' = 0)$, while simultaneously monitoring the resulting fluorescence from diagonal decays. In both cases, excitation is provided via a tunable pulsed dye laser, and the resulting fluorescence is coupled into a grating monochromator and detected using a photomultiplier tube. Compared to previous measurements, 15,17 improvements, such as better source handling

techniques to reduce the production of alkaline earth oxide contaminants, provided an increase in signal-to-noise ratio (SNR) of \sim 3×. This improved SNR enabled spectrometer measurements with a higher resolution of 0.20 nm. Additional experimental details and theoretical methods are provided in the Supporting Information.

Using this improved resolution, we recorded DLIF spectra for the $\tilde{A} \to \tilde{X}$ and $\tilde{B} \to \tilde{X}$ transitions of CaOPh, shown as the red lines in Figures 2a and 2b, respectively. For comparison, the previously recorded DLIF spectra for this molecule 15 are shown as black lines. Several improvements are immediately clear. First, spectral contamination by CaOH molecules, features denoted by asterisks, is greatly reduced. Second, while in the previous work three fundamental vibrational modes (ν_2, ν_4) and ν_9 were resolved within the frequency range of \sim 660 cm⁻¹ below the respective 0–0 transition, the improved measurements here reveal several new features which were either unresolved in or below the detection limit of the previous measurement. Specifically, the lowest-frequency outof-plane bending mode ν_2 (Figure 2d) is much better resolved at a frequency shift of -60 cm⁻¹ (Figures 2a and 2b). A new weak decay is also observed at -241 cm⁻¹ (Figure 2b) and readily assigned to the fundamental out-of-plane bending mode ν_3 (Figure 2d). Further, the previously assigned peaks due to decays to the Ca-O stretching modes ν_4 and ν_9 are seen to be doublets. While theoretical calculations within the harmonic approximation predict that ν_4 should be the strongest off-diagonal decay ($\Delta \nu \neq 0$) (Table S3), the weaker peak at -295 cm⁻¹ is not readily assignable. Compared with the theoretical harmonic vibrational frequencies, the weak peak is near the combination modes $\nu_1 + \nu_3$ and $\nu_2 + \nu_3$, as shown in Figure 2d. However, the predicted Franck-Condon factors (FCFs) for these decays are <10⁻⁴, well below the current detection limit. The observed decay can be explained by an intensity borrowing mechanism, ^{29,30} which arises from anharmonic coupling between the nearly degenerate stretching mode ν_4 and the combination mode consisting of two bending modes, also known as a Fermi resonance. 21,27,28 To corroborate Fermi resonance doublets, vibrational perturbation theory (VPT)31-35 was applied on top of anharmonic frequency calculations to predict corrected frequencies and resonance doublets and obtain anharmonic FCFs (see Supporting Information for more details). As seen in the insets of Figures 2a and 2b, the predicted separations (vertical blue lines) agree well with the observed vibrational doublets (red traces). Given the requirement that coupled vibrational modes have the same symmetry, the weaker peak is attributed to the combination mode $\nu_2 + \nu_3$ with A₁ symmetry, rather than $\nu_1 + \nu_3$ with A_2 symmetry (Figure 2d). Similarly, the doublet near ν_9 is interpreted as a result of vibrational decays to a fundamental mode ν_9 , as observed previously, 15 and the overtone of the stretching mode ν_4 . In the harmonic approximation (Table S3), the decay intensity of ν_9 is relatively consistent between $A \to X$ and $B \to X$ transitions, whereas $2\nu_4$ exhibits significant variation. The decay from A gives a higher intensity for $2\nu_4$, attributed to a larger overlap of vibrational displacement of ν_4 with the in-plane orbital of the \tilde{A} state (Figure 1b). Consequently, this results in an intensity ratio of $\nu_9/2\nu_4$ being four times in the $A \to X$ and ten times in the $B \to X$ transition. The observed nearly equal intensities in both transitions in Figures 2a and 2b are due to the intensity borrowing via the Fermi resonance.

The presence of vibrational doublets due to anharmonic couplings is also observed in the electronically excited \tilde{A} and \tilde{B} states by excitation spectroscopy, as presented in Figure 2c. Here, it is seen that for both electronically excited states, as in the ground state, the Fermi resonance leads to activation of the combination mode $\nu_2 + \nu_3$ at a spacing of around 16 cm⁻¹ from the ν_4 vibrational level (Table S5). Similarly, excitations to the excited vibrational levels of ν_9 and $2\nu_4$, as well as a very weak resonance to the combination band of $\nu_2 + \nu_3 + \nu_4$, are observed. The observation of the vibrational anharmonic coupling across different electronic states highlights the significance of Fermi resonances in the spectral characteristics of large molecules like CaOPh.

To explore the universality of Fermi resonances, we extended our study to the substituted molecules CaOPh-4-F, CaOPh-3-F, and CaOPh-3,4,5-F₃. In Figures 3 and S4, the DLIF spectra of the $\tilde{A} \to \tilde{X}$ and $\tilde{B} \to \tilde{X}$ transitions for these substituted molecules are presented. Remarkably, with a single fluorine atom substituted at the para-position of the phenyl ring, the DLIF spectra of CaOPh-4F (Figures 3a and 3b) show only a single peak for the vibrational decay to the stretching mode ν_4 for both transitions. This implies the absence of a Fermi resonance, which can be attributed to the substantial frequency spacing of 64 cm⁻¹ (harm.) or 69 cm⁻¹ (VPT) between ν_4 and the symmetry-allowed combination band of ν_1 + ν_3 (Figure 3e). Furthermore, the insets in Figures 3a and 3b reveal two weak peaks at frequencies of around -53 cm⁻¹ and -346 cm^{-1} , which can be assigned to modes ν_2 and $\nu_2 + \nu_4$, respectively, by comparing with theoretical frequencies (Figure 3e). These weak peaks are likely due to the anharmonic modecoupling involving the low-frequency bending mode ν_2 . Additionally, the complex peaks observed at around -150cm⁻¹ result from collision-induced relaxation from $\tilde{B} \rightarrow \tilde{A}$, followed by fluorescence decay to the \tilde{X} state, and a vibrational decay to mode ν_3 at -170 cm⁻¹.

In the case of CaOPh-3-F, where para-F is replaced with a meta-F and the molecular symmetry is reduced from $C_{2\nu}$ to $C_{3\nu}$ the coupling phenomenon is markedly different. While previous DLIF studies¹⁵ of $\tilde{A} \to \tilde{X}$ and $\tilde{B} \to \tilde{X}$ transitions found a broad peak for the stretching mode peak ν_5 at -290 cm⁻¹ (black traces in Figures 3c-d), the present, higher resolution spectra, resolve three separate transitions, which are also predicted by the VPT calculation (blue lines in Figures 3cd). The strongest peak at -284 cm⁻¹ corresponds to the vibrational decay to the stretching mode ν_5 (A', Figure 3f), while the other two peaks at -291 cm⁻¹ and -302 cm⁻¹ are assigned to two combination levels, $\nu_2 + \nu_3$ (A') and $\nu_2 + \nu_4$ (A'), respectively. This more complex coupling behavior can be attributed to the lower C_s symmetry of the CaOPh-3-F molecule. All three vibrational modes, ν_2 , ν_3 and ν_4 , are out-ofplane bending modes with A'' symmetry. The combination levels of ν_2 + ν_3 or ν_2 + ν_4 results in A' symmetry and frequencies close to that of the stretching mode ν_5 (Figure 3f), leading to intensity borrowing and activation of these unexpected combination bands.

The absence of a Fermi resonance in the CaOPh-4-F stretching mode decay and the presence of complex coupling in CaOPh-3-F are further supported by the excitation spectra obtained for the excited states. Figure S2 demonstrates a single peak corresponding to the stretching mode ν_4 in the excitation spectra of CaOPh-4-F, while the excitation spectra of CaOPh-3-F (Figure S3) reveal the presence of three transitions in the frequency region associated with the stretching mode ν_5 .

A more complex molecule with three F atoms substituted, CaOPh-3,4,5-F₃, has also been revisited as it is potentially the most attractive calcium phenoxide for optical cycling. ¹⁵ The DLIF spectra in Figure S4 and excitation spectra of excited states in Figure S5 both reveal the presence of doublet vibrational peaks near the stretching mode peak region. One of these peaks corresponds to the stretching mode ν_6 with an A₁ symmetry, while the other peak arises from a combination band involving two out-of-plane bending modes ν_1 (B₁) and ν_4 (B₁).

To investigate the influence of metal atom on anharmonic vibrational coupling, we also studied two strontium phenoxides, SrOPh and SrOPh-3,4,5-F₃. Previous study ¹⁷ has provided low-resolution DLIF spectra for these molecules. Figures 4a and 4b displays the higher resolution DLIF spectra recorded here for SrOPh from the excited \tilde{A} and \tilde{B} states. Only a single transition is observed for stretching mode ν_3 at around –235 cm⁻¹, indicating the lack of Fermi resonance. The absence can be explained by the different symmetry of the combination level of $\nu_1 + \nu_2$ (A₂) and the stretching mode ν_3 (A₁), along with a substantial energy gap of either 130 cm⁻¹

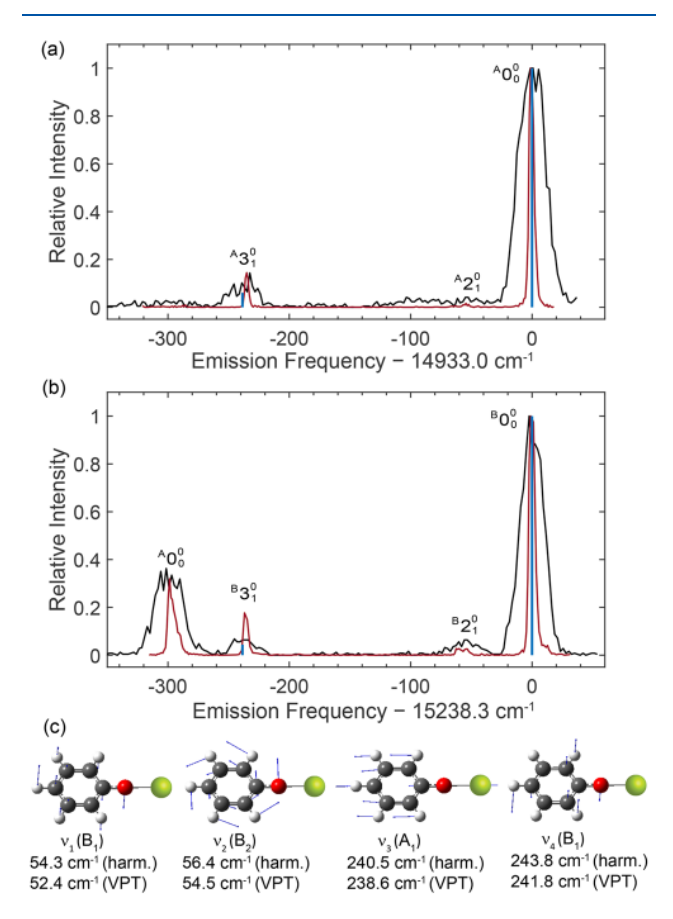


Figure 4. (a, b) DLIF spectra obtained for the $\tilde{A} \to \tilde{X}$ and $\tilde{B} \to \tilde{X}$ transitions of SrOPh molecules. The black traces are taken from a previous study, 17 measured with a spectral resolution of \approx 0.5 nm, while the red traces represent an improved measurement with a resolution of \approx 0.20 nm. The blue sticks show the calculated frequency (VPT) and relative strength (harm) of vibrational decays. (c) Vibrational displacements of four lowest-frequency fundamental modes. Theoretical frequencies and symmetries for these modes are provided. All vibrational modes are labeled with increasing frequency regardless of their symmetries.

(harm.) or 132 cm⁻¹ (VPT), as shown in Figure 4c. This is also validated by the presence of a single stretching mode transition in the excitation spectra of $\tilde{A} \leftarrow \tilde{X}$ and $\tilde{B} \leftarrow \tilde{X}$ in Figure S6.

Contrary to SrOPh, both DLIF spectra (Figure S7) and excitation spectra (Figure S8) of SrOPh-3,4,5-F₃ exhibit a weak transition assigned to the $\nu_1 + \nu_3$ combination mode close to the stretching mode peak ν_4 , implying the existence of a small anharmonic coupling, as also captured by the VPT calculation.

The branching ratios and frequencies of all observed vibrational modes in the DLIF and excitation spectra are summarized in Tables S3–S6. From these, a consistent understanding of the role of vibrational coupling in the calcium and strontium phenoxide molecules emerges. As summarized in Tables 1, S3, and S4, except for CaOPh-4-F and SrOPh molecules, all examined molecules show additional off-diagonal decays near the most off-diagonal decays to the stretching mode (ν_k). Specifically, a combination band ($\nu_i + \nu_j$) comprising two low-frequency bending modes, which is absent in the harmonic approximation, is activated by anharmonic vibrational coupling. This occurs in a predictable manner according to the vibrational frequency spacing and vibrational mode symmetry and can be captured by the VPT calculations.

The strength of this coupling can be estimated from an intensity borrowing model in a molecular system with effects of anharmonicity.³⁶ Following the convention, the anharmonic vibrational Hamiltonian is expressed as

$$H_{anh}^{(\tilde{X})} = \frac{1}{6} \sum_{i,j,k} \left(\frac{\partial^3 V^{(\tilde{X})}}{\partial Q_i \partial Q_j \partial Q_k} \right)_0 Q_i Q_j Q_k + ..., \tag{1}$$

where the higher-order anharmonic terms in the vibrational potential energy in the \tilde{X} state $(V^{(\tilde{X})})$ are negelected. By rewriting the normal coordinates Q_i , Q_j and Q_k with the annihilation and creation operators for the vibration modes, e.g., $Q_i = 1/\sqrt{2(\hat{a}_i^{\dagger} + \hat{a}_i)^{37}}$ the Fermi resonance Hamiltonian affecting the combination mode $\nu_i + \nu_j$ and fundamental mode ν_k in the ground \tilde{X} state can be expressed as

$$H_{FR,ij,k}^{(\tilde{X})} = \phi_{ij,k}^{(\tilde{X})}(\hat{a}_{i}^{\dagger}\hat{a}_{j}^{\dagger}\hat{a}_{k} + \hat{a}_{i}\hat{a}_{j}\hat{a}_{k}^{\dagger})$$
(2)

where $\phi_{ij,k}^{(\tilde{X})}$ is the coupling strength. In the absence of the Fermi resonance (i.e., $\phi_{ij,k}^{(\tilde{X})}=0$), we assume the probability of decay from the excited state $|e, \nu'=0\rangle$ to $|\tilde{X}, \nu_k''\rangle$ (denoted as $I_{e0,X\nu_k}$) is appreciable, while decay to the combination mode $|\tilde{X}, \nu_i'' + \nu_j''\rangle$ (denoted as $I_{e0,X\nu_{\nu_j}}$) is negligible. As $\phi_{ij,k}^{(\tilde{X})} \neq 0$, the extra and main line intensities can be presented as

$$I'_{e0,X\nu_{i}\nu_{j}} = (C_{k,ij}^{(X)})^{2} I_{e0,X\nu_{k}}$$
(3)

and

$$I'_{e0,X\nu_k} = [1 - (C_{k,ij}^{(X)})^2] I_{e0,X\nu_k}$$
(4)

respectively, where the coefficient $(C_{k,ij}^{(X)})^2$ is the ratio of the borrowed intensity. In the experiment, the ratio of the two intensities is measured, i.e., $\beta_{k/ij} = I'_{e0,X\nu_k}/I'_{e0,X\nu_{\nu_i}} = (C_{k,ij}^{(X)})^{-2} - 1$. Treating the case of only one combination mode mixing with the stretching mode as a simple two level system, one can obtain

Table 1. Summary of the Fermi Resonance for the Most Off-Diagonal Decays to the Stretching Modes in All Studied Molecules^a

	Theo. (VPT)					Exp.		
Species	ν_i	$ u_j$	ν_k	$\Delta u^{(0)}_{ij,k}$	$\Delta u_{ij,k}$	$\Delta u'_{ij,k}$	$oldsymbol{eta}_{k/ij}$	$oldsymbol{\phi}_{ij,k}^{(ilde{X})}$
CaOPh	60.0 (B ₁ , ν_2)	241.0 (B ₁ , ν_3)	315.2 (A_1, ν_4)	14.2	19.6	18.0(0.4)	2.9(0.8)	7.9(0.6)
CaOPh-3-F	57.9 (A", ν_2)	234.5 (A", ν_3)	286.0 (A', ν_5)	6.4	8.2	6.1(0.6)	3.0(1.0)	_
	57.9 (A", ν_2)	242.3 (A", ν_4)	286.0 (A', ν_5)	14.2	16.0	17.4(0.6)	1.9(0.4)	_
CaOPh-3,4,5-F ₃	48.9 (B ₁ , ν_1)	217.2 (B ₁ , ν_4)	271.2 (A_1, ν_6)	5.1	9.6	8.2(0.4)	1.0(1.0)	4.2(2.4)
SrOPh-3,4,5-F ₃	45.7 (B ₁ , ν_1)	143.6 (B ₁ , ν_3)	203.5 (A_1, ν_4)	14.2	16.2	18.7(1.0)	9.0(4.0)	6.0(2.6)
CaOPh-4-F	48.6 (B ₁ , ν_1)	171.0 (B ₁ , ν_3)	288.5 (A ₁ , ν_4)	68.9	None	No doublet observed		
SrOPh	52.4 (B ₁ , ν_1)	54.5 (B ₂ , ν_2)	238.6 (A ₁ , ν_3)	131.7	None	No doublet observed		

a Notes: ν_i and ν_j are two low-frequency out-of-plane bending modes. The combination band of $\nu_i + \nu_p$ FCF-inactive mode under harmonic approximation, is likely to show up due to the intensity borrowing from Fermi resonance coupling with the most-off diagonal decays to the stretching mode ν_k based on the frequency spacing and symmetry. $\Delta\nu_{ij,k}^{(0)} = |\nu_k - \nu_i - \nu_j|$ is the unperturbed frequency separation, and $\Delta\nu_{ij,k} = |\nu_k - \nu_i - \nu_j|$ are the predicted Fermi resonance doublets ("None" indicates no Fermi resonance predicted for the mode ν_k). The difference of $|\Delta\nu_{ij,k}^{(0)} - \nu_j|$ $\Delta
u_{ij,k}$ indicates the frequency shift due to Fermi resonance. All frequencies are calculated at the anharmonic-VPT level of theory. $\Delta
u_{ij,k}$ is the measured frequency spacing between the combination band and the stretching mode. $\beta_{k/ij}$ is the averaged measured peak intensity ratio of the stretching mode to the combination band in $\tilde{A} \to \tilde{X}$ and $\tilde{B} \to \tilde{X}$ transitions. $\phi_{ij,k}^{(\tilde{X})}$ is the estimated Fermi resonance coupling strength between the combination band and the stretching mode in the ground state according to eq 6. Due to the complexity of coupling between multiple vibrational bands, the coupling strength of CaOPh-3-F could not be estimated from the measurement. All frequencies and coupling strengths are given in units

$$C_{k,ij}^{(X)} = \sqrt{\frac{1}{2} \left(1 - \frac{\Delta \nu_{ij,k}^{(0)}}{\Delta \nu_{ij,k}'} \right)}$$
 (5)

and

$$\phi_{ij,k}^{(\tilde{X})} = \frac{\sqrt{\beta_{k/ij}}}{\beta_{k/ij} + 1} \Delta \nu_{ij,k}'$$
(6)

where $\Delta
u_{ii.k}^{(0)}$ is the unperturbed energy gap between the modes. Using this expression, coupling strengths are extracted and are shown in Table 1. For this comparison, although the unperturbed gap $\Delta \nu_{ij,k}^{(0)}$ could be evaluated from the measurement $(\beta_{k/ij})$ and $\Delta \nu_{ij,k}^{(0)}$ and the above equations, we employ the calculated VPT frequencies for a straightforward comparison of calculated and measured gaps.

Although Fermi resonance occurring between multiple vibrational modes (ν_5 , ν_2 + ν_3 , and ν_2 + ν_4) is observed in CaOPh-3-F, evaluating the anharmonic coupling strengths between these modes is challenging. This is due to the mismatch between the numbers of independent elements and available observables: we represent the three-level system with a 3 × 3 matrix, containing six independent elements, but only have five observables (three frequencies and two relative intensity ratios). Such mismatch results in nonunique solutions from the intensity borrowing model, leading to significant uncertainties in the matrix elements. As a result, the measurement of the coupling coefficients of CaOPh-3-F is not available in Table 1.

The observed anharmonic couplings have substantial implications for the laser cooling of these molecules. The presence of additional vibrational decay pathways requires the use of additional repumping lasers to achieve efficient photon scattering.²³⁻²⁵ Therefore, it is crucial to design molecules that can minimize or avoid such resonant couplings. Several such strategies for mitigating vibrational anharmonic coupling are readily apparent in these molecules. First, the spacing of vibrational energy levels can be tailored to maintain sufficient separation of harmonic states to avoid detrimental Fermi resonances. This can be achieved via several approaches, such as substituting groups on the phenyl ring (e.g., CaOPh-4-F) or altering the metal atom hosting the optical cycling center (e.g., SrOPh). For example, according to theoretical calculations, it is anticipated that CaOPh-4-Cl, CaOPh-4-OH, SrOPh-3-F, and SrOPh-3-OH will not exhibit Fermi resonance coupling between the stretching mode and the bending mode combination band due to their large frequency spacings (>60 cm⁻¹, Table S7). Second, choosing molecules with higher symmetry may protect the stretching mode from mixing with other nearby combination modes, as the Fermi resonance only affects modes in the same symmetry.

As the molecular size and complexity increase above the molecules studied here, the increased density of vibrational states from the increasingly diverse molecular structure will pose challenges for the effectiveness of the mitigation methods discussed here. Selecting suitable ligands with a strong electron-withdrawing capability can offer a general suppression of Fermi resonance and higher order couplings. For these molecules, as the orbital motion of the electrons is highly separated from the vibrational degrees of freedom, 8,15 the anharmonic effects induced by these molecular orbitals can be mitigated; therefore, the couplings relative to the most offdiagonal decays are suppressed.

In summary, we have studied the Fermi resonance coupling of calcium and strontium phenoxides and their derivatives, employing high-resolution dispersed laser-induced fluorescence and excitation spectroscopy. Fermi resonance phenomena were observed in the ground and excited states for CaOPh, CaOPh-3,4,5-F₃, and SrOPh-3,4,5-F₃ molecules. This resonance led to intensity borrowing, particularly in vibrational combination bands consisting of two low-frequency bending modes close in energy to a stretching mode. The Fermi resonance effect was absent in CaOPh-4-F and SrOPh due to large frequency differences between the combination band and the stretching mods. While Fermi resonance does not significantly alter vibrational branching ratios, it does require additional repumping lasers for effective optical cycling. Several strategies were presented to minimize the impact of Fermi resonance on phenoxide-related molecules, including ligand substitutions and changes in metal atoms. These

findings help to provide a roadmap for the design and engineering of ever-larger and more intricate molecular systems with enhanced optical cycling properties for advancing quantum information science.

ASSOCIATED CONTENT

Supporting Information

The Supporting Information is available free of charge at https://pubs.acs.org/doi/10.1021/acs.jpclett.3c03177.

Experimental and theoretical methods, error analysis of vibrational branching ratios, Tables S1–S8 (including summaries of vibrational branching ratios and frequencies of all resolved vibrational modes), and Figures S1–S8 (including DLIF and excitation spectra of all other molecules) (PDF)

Transparent Peer Review report available (PDF)

AUTHOR INFORMATION

Corresponding Author

Guo-Zhu Zhu — Department of Physics and Astronomy, University of California, Los Angeles, California 90095, United States; ⊚ orcid.org/0000-0002-5635-3679; Email: guozhu.zhu@physics.ucla.edu

Authors

Guanming Lao – Department of Physics and Astronomy, University of California, Los Angeles, California 90095, United States

Claire E. Dickerson — Department of Chemistry and Biochemistry, University of California, Los Angeles, California 90095, United States; orcid.org/0000-0001-7617-9287

Justin R. Caram — Department of Chemistry and Biochemistry and Center for Quantum Science and Engineering, University of California, Los Angeles, California 90095, United States; orcid.org/0000-0001-5126-3829

Wesley C. Campbell – Department of Physics and Astronomy, Center for Quantum Science and Engineering, and Challenge Institute for Quantum Computation, University of California, Los Angeles, California 90095, United States

Anastassia N. Alexandrova — Department of Chemistry and Biochemistry and Center for Quantum Science and Engineering, University of California, Los Angeles, California 90095, United States; orcid.org/0000-0002-3003-1911

Eric R. Hudson — Department of Physics and Astronomy, Center for Quantum Science and Engineering, and Challenge Institute for Quantum Computation, University of California, Los Angeles, California 90095, United States

Complete contact information is available at: https://pubs.acs.org/10.1021/acs.jpclett.3c03177

Notes

The authors declare no competing financial interest.

ACKNOWLEDGMENTS

This work was supported by the AFOSR (Grant No. FA9550-20-1-0323), the NSF (Grant Nos. OMA-2016245, PHY-2207985, and DGE-2034835), NSF Center for Chemical Innovation Phase I (Grant No. CHE-2221453) and the Gordon and Betty Moore Foundation (DOI: 10.37807/GBMF11566). Computational resources were provided by

ACCESS and UCLA IDRE. C.E.D. thanks Mark Boyer for helpful discussions.

REFERENCES

- (1) Isaev, T. A.; Berger, R. Polyatomic Candidates for Cooling of Molecules with Lasers from Simple Theoretical Concepts. *Phys. Rev. Lett.* **2016**, *116*, 063006.
- (2) Kozyryev, I.; Baum, L.; Matsuda, K.; Doyle, J. M. Proposal for Laser Cooling of Complex Polyatomic Molecules. *ChemPhysChem* **2016**, *17*, 3641–3648.
- (3) Ivanov, M. V.; Bangerter, F. H.; Krylov, A. I. Towards a Rational Design of Laser-Coolable Molecules: Insights from Equation-of-Motion Coupled-Cluster Calculations. *Phys. Chem. Chem. Phys.* **2019**, 21, 19447—19457.
- (4) Ivanov, M. V.; Gulania, S.; Krylov, A. I. Two Cycling Centers in One Molecule: Communication by Through-Bond Interactions and Entanglement of the Unpaired Electrons. *J. Phys. Chem. Lett.* **2020**, *11*, 1297–1304.
- (5) Ivanov, M. V.; Bangerter, F. H.; Wójcik, P.; Krylov, A. I. Toward Ultracold Organic Chemistry: Prospects of Laser Cooling Large Organic Molecules. *J. Phys. Chem. Lett.* **2020**, *11*, 6670–6676.
- (6) Klos, J.; Kotochigova, S. Prospects for Laser Cooling of Polyatomic Molecules with Increasing Complexity. *Phys. Rev. Res.* **2020**, *2*, 013384.
- (7) Augenbraun, B. L.; Doyle, J. M.; Zelevinsky, T.; Kozyryev, I. Molecular Asymmetry and Optical Cycling: Laser Cooling Asymmetric Top Molecules. *Phys. Rev. X* **2020**, *10*, 031022.
- (8) Dickerson, C. E.; Guo, H.; Shin, A. J.; Augenbraun, B. L.; Caram, J. R.; Campbell, W. C.; Alexandrova, A. N. Franck-Condon Tuning of Optical Cycling Centers by Organic Functionalization. *Phys. Rev. Lett.* **2021**, *126*, 123002.
- (9) Dickerson, C. E.; Guo, H.; Zhu, G.-Z.; Hudson, E. R.; Caram, J. R.; Campbell, W. C.; Alexandrova, A. N. Optical Cycling Functionalization of Arenes. *J. Phys. Chem. Lett.* **2021**, *12*, 3989–3995.
- (10) Paul, A. C.; Sharma, K.; Telfah, H.; Miller, T. A.; Liu, J. Electronic Spectroscopy of the \tilde{A}_1 $^2A''/\tilde{A}_2$ $^2A' \tilde{X}$ $^2A'$ Transitions of Jet-Cooled Calcium Ethoxide Radicals: Vibronic Structure of Alkaline Earth Monoalkoxide Radicals of C_s Symmetry. *J. Chem. Phys.* **2021**, 155, 024301.
- (11) Telfah, H.; Sharma, K.; Paul, A. C.; Riyadh, S. S.; Miller, T. A.; Liu, J. A Combined Experimental and Computational Study on the Transition of the Calcium Isopropoxide Radical as a Candidate for Direct Laser Cooling. *Phys. Chem. Chem. Phys.* **2022**, *24*, 8749–8762.
- (12) Dickerson, C. E.; Chang, C.; Guo, H.; Alexandrova, A. N. Fully Saturated Hydrocarbons as Hosts of Optical Cycling Centers. *J. Phys. Chem. A* **2022**, *126*, 9644–9650.
- (13) Yu, P.; Lopez, A.; Goddard, W. A.; Hutzler, N. R. Multivalent Optical Cycling Centers: Towards Control of Polyatomics with Multi-Electron Degrees of Freedom. *Phys. Chem. Chem. Phys.* **2022**, 25, 154–170.
- (14) Sinenka, H.; Bruyakin, Y.; Zaitsevskii, A.; Isaev, T.; Bochenkova, A. V. Zwitterions Functionalized by Optical Cycling Centers: Toward Laser-Coolable Polyatomic Molecular Cations. *J.Phys. Chem. Lett.* **2023**, *14*, 5784–5790.
- (15) Zhu, G.-Z.; Mitra, D.; Augenbraun, B. L.; Dickerson, C. E.; Frim, M. J.; Lao, G.; Lasner, Z. D.; Alexandrova, A. N.; Campbell, W. C.; Caram, J. R.; et al. Functionalizing Aromatic Compounds with Optical Cycling Centers. *Nat. Chem.* **2022**, *14*, 995–999.
- (16) Mitra, D.; Lasner, Z. D.; Zhu, G.-Z.; Dickerson, C. E.; Augenbraun, B. L.; Bailey, A. D.; Alexandrova, A. N.; Campbell, W. C.; Caram, J. R.; Hudson, E. R.; et al. Pathway Towards Optical Cycling and Laser Cooling of Functionalized Arenes. *J. Phys. Chem. Lett.* 2022, 13, 7029–7035.
- (17) Lao, G.; Zhu, G.-Z.; Dickerson, C. E.; Augenbraun, B. L.; Alexandrova, A. N.; Caram, J. R.; Hudson, E. R.; Campbell, W. C. Laser Spectroscopy of Aromatic Molecules with Optical Cycling Centers: Strontium (I) Phenoxides. *J. Phys. Chem. Lett.* **2022**, *13*, 11029–11035.

- (18) Changala, P. B.; Genossar-Dan, N.; Brudner, E.; Gur, T.; Baraban, J. H.; McCarthy, M. C. Structural and Electronic Trends of Optical Cycling Centers in Polyatomic Molecules Revealed by Microwave Spectroscopy of MgCCH, CaCCH, and SrCCH. *Proc. Natl. Acad. Sci. U.S.A.* 2023, 120, e2303586120.
- (19) Guo, H.; Dickerson, C. E.; Shin, A. J.; Zhao, C.; Atallah, T. L.; Caram, J. R.; Campbell, W. C.; Alexandrova, A. N. Surface Chemical Trapping of Optical Cycling Centers. *Phys. Chem. Chem. Phys.* **2021**, 23, 211–218.
- (20) Uzer, T.; Miller, W. Theories of Intramolecular Vibrational Energy Transfer. *Phys. Rep.* **1991**, *199*, 73–146.
- (21) Nesbitt, D. J.; Field, R. W. Vibrational Energy Flow in Highly Excited Molecules: Role of Intramolecular Vibrational Redistribution. *J. Phys. Chem.* **1996**, *100*, 12735–12756.
- (22) Keske, J. C.; Pate, B. H. Decoding the Dynamical Information Embedded in Highly Mixed Quantum States. *Annu. Rev. Phys. Chem.* **2000**, *51*, 323–353.
- (23) McCarron, D. Laser Cooling and Trapping Molecules. J. Phys. B: At. Mol. Opt. Phys. 2018, 51, 212001.
- (24) Fitch, N.; Tarbutt, M. Laser-Cooled Molecules. *Advances In Atomic, Molecular, and Optical Physics* **2021**, *70*, 157–262.
- (25) Augenbraun, B. L.; Anderegg, L.; Hallas, C.; Lasner, Z. D.; Vilas, N. B.; Doyle, J. M. Direct laser cooling of polyatomic molecules. *Advances in Atomic, Molecular, and Optical Physics* **2023**, 72, 89–182.
- (26) Augenbraun, B. L.; Burchesky, S.; Winnicki, A.; Doyle, J. M. High-Resolution Laser Spectroscopy of a Functionalized Aromatic Molecule. *J. Phys. Chem. Lett.* **2022**, *13*, 10771–10777.
- (27) Fermi, E. Über den Ramaneffekt des Kohlendioxyds. Z. Phys. 1931, 71, 250–259.
- (28) Dübal, H.-R.; Quack, M. Tridiagonal Fermi Resonance Structure in the IR Spectrum of the Excited CH Chromophore in CF₃H. *J. Chem. Phys.* **1984**, *81*, 3779–3791.
- (29) Zhang, C.; Augenbraun, B. L.; Lasner, Z. D.; Vilas, N. B.; Doyle, J. M.; Cheng, L. Accurate Prediction and Measurement of Vibronic Branching Ratios for Laser Cooling Linear Polyatomic Molecules. J. Chem. Phys. 2021, 155, 091101.
- (30) Zhang, C.; Hutzler, N. R.; Cheng, L. Intensity-Borrowing Mechanisms Pertinent to Laser Cooling of Linear Polyatomic Molecules. *J. Chem. Theory Comput.* **2023**, *19*, 4136–4148.
- (31) Nielsen, H. H. The Vibration-Rotation Energies of Molecules. *Rev. Mod. Phys.* **1951**, 23, 90.
- (32) Barone, V. Anharmonic Vibrational Properties by a Fully Automated Second-Order Perturbative Approach. *J. Chem. Phys.* **2005**, *122*, 014108.
- (33) Boyer, M. A.; McCoy, A. B. PyVibPTn, a General Package for Vibrational Perturbation Theory. *Zenodo*. 2021, DOI: 10.5281/zenodo.5563091.
- (34) Boyer, M. A.; McCoy, A. B. Flexible Approach to Vibrational Perturbation Theory Using Sparse Matrix Methods. *J. Chem. Phys.* **2022**, *156*, 054107.
- (35) Boyer, M. A.; McCoy, A. B. Wave Function Correction-Based Approach to the Identification of Resonances for Vibrational Perturbation Theory. *J. Chem. Phys.* **2022**, *157*, 164113.
- (36) Atkins, P. W.; Friedman, R. S. Molecular Quantum Mechanics; Oxford University Press: 2011.
- (37) Lefebvre-Brion, H.; Field, R. W. The Spectra and Dynamics of Diatomic Molecules; Elsevier: 2004.